Numerical Simulation of Laminar Flow Over a Transversely Oscillating Circular Cylinder

Ussama Ali [a, b], Ayoola Brimmo [a], Md Islam [a], Isam Janajreh [a] *

[a] *Department of Mechanical Engineering, Khalifa University of Science and Technology, Abu Dhabi, UAE*
[b] *Department of Mechanical Engineering, University of Engineering and Technology, Lahore, 54890, Pakistan*

Abstract

Two-dimensional low Reynolds number flow (Re = 100) over a transversely oscillating circular cylinder placed in a uniform stream is numerically investigated in this work using the commercial software Ansys/Fluent. The forced transverse oscillations of the cylinder are carried out to mimic the specific cases of flow-induced vibrations. The frequency ratio is varied between 0 – 2, where 0 corresponds to stationary cylinder. The layering technique of dynamic mesh is employed to incorporate the cylinder motion. The unsteady flow simulations are performed to solve for URANS. The parameters studied are the coefficients of lift and drag, vortex shedding frequency, and the vortex shedding patterns. The results reveal that the cylinder oscillation induces modulation in the lift and drag coefficients in terms of their frequency and amplitude. The lock-in occurs at frequency ratio of 1 where the frequency of cylinder oscillation matches with the natural vortex shedding frequency of the cylinder. Maximum average drag coefficient is observed at the lock-in condition however the lift coefficient is found to increase with the frequency ratio. The 2S vortex shedding pattern is observed in the vorticity contours for all the cases studied.

Keywords: Forced transverse oscillations, Unsteady flow, Lift and drag coefficients, Vortex shedding pattern

1. Introduction

External flow around bodies such as the airfoil and cylinder has been studied extensively due to the immense practical value [1]. The flow dynamics can be changed by changing the flow conditions [2], geometric parameters [3], or by passive or active control techniques [4]. As an example, the airfoils are made streamlined to increase the lift and reduce the drag [5, 6, 7]. Splitter plates, surface roughness, or creating a slit are one of the few passive control techniques for cylinders [8, 9]. Viscous flow around a cylinder leads to periodic flow separation from lateral sides of the cylinder leading to von Karman vortex street for Reynolds number (Re) as low as 47 [10]. The vortex shedding depends on various parameters such as the Re, shape of the cylinder, cylinder motion etc. The frequency of shedding can be mapped as a function of Re in the laminar regime [11]. The cylinder wake transformers from 3D to 2D for Re = 190 – 260 [12].

The periodic vortex shedding induces periodic aerodynamic/hydrodynamic forces on the body (lift and drag). This can lead to the vibration of the structure and these vibrations can be fatal if the frequency of vortex shedding matches with that of the structure's natural frequency. This condition is known as the lock-in [13, 14]. The mystery of forecasting the behavior of bodies undergoing flow-induced vibrations (FIV) has puzzled engineers for a long time. The examples of FIV can be found in marine towing cables, chimney stacks, power transmission lines, offshore drilling platforms, cables of bridges, etc. The non-linearity between the forcing function and the behavior of the body adds to the complexity of the problem [15]. The movement of the structure affects the wake flow which in turn affects the forces acting on the body. To study such responses, researchers have performed experimental as well as numerical studies. A large amount of literature is available on this topic out of which few works are highlighted here. FIV can occur in transverse as well as streamwise direction. However, as the transverse direction FIV

is more severe and occur more frequently, therefore in this study only transverse motion of the cylinder will be studied.

Wanderley and Soares [16] analyzed the transverse FIV of a single cylinder numerically. Effect of *Re* on the cylinder response behavior was studied. They reported that the cylinder response was strongly affected by the *Re*. In their study, maximum vibration of the cylinder was 0.55*D* where *D* was the cylinder's diameter. Bernitsas and Raghavan [17] experimentally studied the FIV of a circular cylinder. They reported that the cylinder vibrational amplitude increased with increase in *Re*. Chung [18] considered a circular cylinder close to a stationary wall. The effect of the distance between the cylinder and the wall was numerically studied at *Re* of 100. In their study it was observed that the presence of a wall increased the drag coefficient on the cylinder.

Taking into consideration the importance and frequent occurrence of FIV in industrial applications, more work needs to be done to fully understand this phenomenon in order to prevent the devastating damage to the equipment and structures. Therefore, in this study the effect of frequency of oscillation on the induced forces, and wake structures will be studied for a circular cylinder in laminar regime. This work will present the layering technique of dynamic meshing to study the flow dynamics behind a transversely oscillating circular cylinder. The two-dimensional (2D) flow across a circular cylinder in the laminar regime at *Re* of 100 will be studied. Specific cases of FIV will be considered and simulated at stipulated frequency ratios (f/f_{vs}). The remaining paper is organized as follows. Section 2 presents the methodology followed to carry out this study. The results of this study are presented and discussed in Section 3. Finally, the conclusions are given in Section 4.

2. Methodology

In this section, the details about the numerical setup are presented which include the computational domain, boundary conditions, governing equations, and the dynamic mesh technique. The mesh independence study and model validation are also presented in this section.

2.1. Computational Domain

The flow domain is depicted in Fig. 1 along with the discretized mesh. The flow domain consists of a rectangular zone with a circular cylinder with a diameter of *D* placed inside it. The upstream distance of the domain from the cylinder center is set at 12*D* to ensure that the flow is stable when it reaches the cylinder. The downstream length of 4*D* led to 15% discrepancy in the accuracy of the results [19]. Therefore, in this study the downstream length of the domain is taken as 32*D* to observe the vortex shedding. The lateral lengths are set as 20*D* to give the blockage ratio of 5% as a higher blockage ratio affects the accuracy of the results [20, 21].
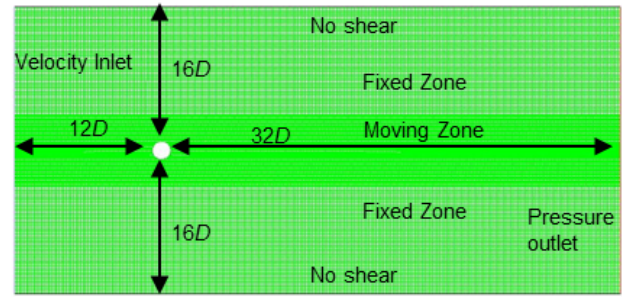

Fig. 1. Computational domain, boundary conditions, and discretized mesh

A structured mesh using quad elements was created as shown in Fig. 1 with 56,832 cells. The cells are finely spaced close to the cylinder wall. As shown in Fig. 1, a horizontal strip of the mesh with height ranging from -4*D* to 4*D* was designated as moving zone. The mesh in this region was very fine. The region above and below this zone was set as fixed zone. The dynamic layering technique was applied to this moving zone to account for the motion of the cylinder. The boundaries between the various regions are conformal. Although, the non-conformal or sliding interface capability in Ansys/Fluent could have been used to connect the various zones in the final model if a non-conformal boundary was specified.

2.2. Boundary Conditions

The assigned boundary conditions are presented in Fig. 1. At the inlet, constant inlet velocity (*U*) is applied such that the flow Reynolds number stays constant at 100. The fluid and the cylinder are assumed at equal and constant temperature. At the outlet zero gage pressure is applied. The lateral walls of the domain are considered as free slip walls with zero shear. The wall of the cylinder is considered as no slip wall and at the same temperature as the incoming fluid.

2.3. Governing Equations

The mathematical equations that describe the fluid flow in this study are presented here. The fluid is considered as incompressible viscous. The fluid properties are considered to be constant as there is no change in the temperature. Therefore, the flow is governed by the continuity equation and the two momentum equations in *x*- and *y*- direction, since only 2D study is carried out. These equations present the conservation of mass and momentum laws. The energy equation is neglected since there is no change in temperature and no heat transfer. The equations in their primitive variable form are presented as follows:

Continuity:

$$\frac{\partial u}{\partial x} + \frac{\partial v}{\partial x} = 0 \qquad (1)$$

x-momentum:

$$\frac{\partial u}{\partial t} + \frac{\partial uu}{\partial x} + \frac{\partial uv}{\partial y} = -\frac{\partial(p/\rho)}{\partial x} + \mu\left(\frac{\partial^2 u}{\partial x^2} + \frac{\partial^2 u}{\partial y^2}\right) \qquad (2)$$

y-momentum:

$$\frac{\partial v}{\partial t} + \frac{\partial uv}{\partial x} + \frac{\partial vv}{\partial y} = -\frac{\partial (p/\rho)}{\partial y} + \mu\left(\frac{\partial^2 v}{\partial x^2} + \frac{\partial^2 v}{\partial y^2}\right) \quad (3)$$

where the velocity components u and v are in the x- and y-directions respectively, μ and ρ are the viscosity and the density of the fluid, respectively, and p is the pressure.

The integral form of the conservation equation for a general scalar ϕ for the dynamic mesh can be written as:

$$\frac{d}{dt}\int_V \rho\varphi dV + \int_{\partial V}\rho\varphi(\bar{u}-\bar{u}_g)d\bar{A} = \int_{\partial V}\mathbf{\Gamma}\nabla\varphi d\bar{A} + \int_V S_\varphi.dV \quad (4)$$

where u is the velocity vector and u_g is the mesh velocity for moving mesh. S_ϕ is the source term, and Γ is the diffusion coefficient. The boundary of the control volume V is represented by ∂V.

The first time on the left-hand side of Eq. 4 can be written, using a 1st-order backward difference scheme, as:

$$\frac{d}{dt}\int_V \rho\varphi dV = \frac{(\rho\varphi V)^{n+1} - (\rho\varphi V)^n}{\Delta t} \quad (5)$$

where n and $n+1$ give the value of the quantity at current and next time step. At $(n+1)$ time, the volume V^{n+1} is calculated as:

$$V^{n+1} = V^n + \frac{dV}{dt}\Delta t \quad (6)$$

where dV/dt represent the time derivative of the volume. It is calculated as:

$$\frac{dV}{dt} = \int_{\partial V}\bar{u}_g.d\bar{A} = \sum_j^{n_f}\bar{u}_{gj}.\bar{A}_j \quad (7)$$

where n_f represent the number of faces on the control volume and A_j is the j face area vector. The dot product $(u_{gj}.A_j)$ is computed from the equation below:

$$\bar{u}_{gj}.\bar{A}_j = \frac{\partial V_j}{\Delta t} \quad (8)$$

where ∂V_j gives the volume swept by the control volume face j over the time step Δt.

The dimensionless Reynolds number (Re) and Strouhal number (St) are defined as follows:

$$Re = \frac{\rho U D}{\mu} \quad (9)$$

$$St = \frac{f_{vs}D}{U} \quad (10)$$

where f_{vs} is the vortex shedding frequency of the stationary cylinder, and U is the freestream velocity.

2.4. Dynamic Mesh Motion

The mesh is created using commercial software Ansys. The numerical solution to the system of equations given in Section 2.3 is obtained via Ansys/Fluent, which is a finite-volume based solver. The dynamic mesh technique in Fluent is used to incorporate the motion of the cylinder. The technique followed here is similar to the one used by Kocabiyiki et al. [22]. The transverse periodic motion of the cylinder makes the unsteady solution in the dynamic mesh simulation time periodic. In this study, the dynamic layering, dynamic mesh module is used to solve the unsteady flow motion. This module allows mesh deformation by removing or adding layers of cells adjacent to the moving boundary. To preserve the quality of the mesh during the cylinder's motion, the ideal layer height (h_{ideal}) on each moving boundary is specified. The layer of cells adjacent to the moving boundary (layer j in Fig. 2) is split or merged, based on the height (h) of the cells in layer j, with the layer of cells next to it (layer i in Fig. 2)
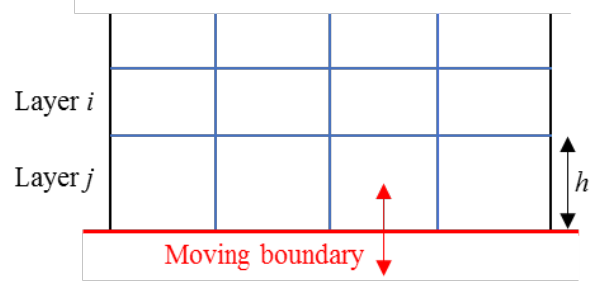

Fig. 2. Dynamic mesh layering technique

To avoid skewness of the computational cells the splitting of the cells during expansion is controlled by a specified split factor (α_{split}). This factor ensures cells are split to create a layer of cells with constant height h_{ideal} and a layer of cells of height $(h-h_{ideal})$ when the criterion of Eq. 11 below is met:

$$h_{min} > (1 + \alpha_{split})h_{ideal} \quad (11)$$

where h_{min} is the minimum cell height of layer j and h_{ideal} is the ideal cell height. A similar model is specified to handle cases of cells compression. The factor α_c ensures cells are compressed until:

$$h_{min} < \alpha_c h_{ideal} \quad (12)$$

where α_c is the collapse factor. When the criteria in Eq. 12 is met, the cells in layer j are merged with those in layer i [23].

The periodic motion of the moving zone in the model was applied using a user-defined function (UDF). At the end of each time step, the force applied to the cylinder is calculated by this subroutine once the time step convergence has been achieved. The transverse motion is calculated with the following equations:

$$Y(t) = A sin(2\pi f t) \quad (13)$$

where Y is the displacement of the cylinder in transverse direction, A is the maximum amplitude of displacement, f is the frequency of motion, and t is the flow time. The unsteady numerical simulation was performed at a time step of 0.0025 to incorporate the cylinder motion and to ensure the Courant–Friedrichs–Lewy (CFL) condition < 1.

2.5. Mesh Independence and Model Validation

The mesh independence is carried out in order to be certain of the quality of the mesh. Four levels of mesh are created as shown in Table 1. The analysis is carried out with the stationary cylinder. The average drag coefficient (C_D) and Strouhal number (St) are evaluated at each mesh and the percentage difference with the fine mesh is calculated. Comparing with the fine mesh, the current mesh with 56,832 number of elements produced 0.63% error in average C_D and 1.16% error in St. The other two mesh (coarse 1 and coarse 2) gave larger error as compared to the current mesh when comparing the values with the fine mesh. As the deviation is very less for the current mesh compared with the results of the fine mesh, therefore the current mesh is selected as a compromise between accuracy and computational time. For further numerical analysis current mesh was used.

Table 1. Mesh sensitivity results

Mesh (number of elements)	Average C_D (-)	Error in avg. C_D %	Strouhal number (St)	Error in St %
Coarse 1 15,308	1.3411	1.69	0.1642	1.48
Coarse 2 29,414	1.3326	1.04	0.16447	1.32
Current Mesh 56,832	1.3272	0.63	0.16473	1.16
Fine 98,628	1.3189	---	0.16667	---

The results obtained through the numerical analysis were also compared with the experimental results of Williamson [24] as shown in Fig. 3. The Re was varied in the range of 50 – 160 and the Strouhal number for the stationary cylinder was recorded. As seen from Fig. 3, the results of this numerical study were in good agreement with those of Williamson [24].
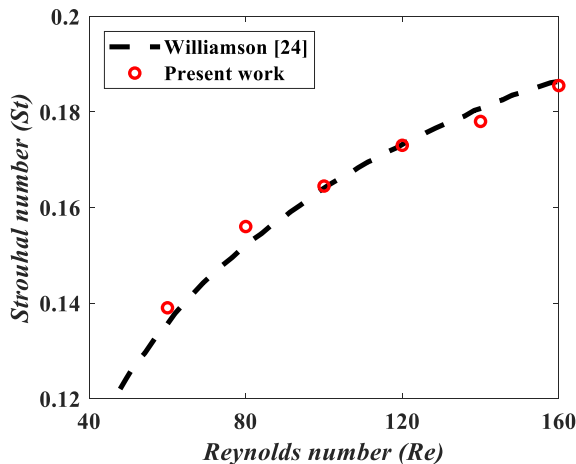

Fig. 3. Validation of results for stationary cylinder with the experimental results of Williamson [24].

3. Results and Discussion

The results of the numerical analysis performed in this study are presented in this section. The frequency of oscillation of cylinder is presented in terms of frequency ratio (f/f_{vs}) where f is the frequency of oscillation of cylinder and f_{vs} is the vortex shedding frequency of stationary cylinder. The time histories of lift coefficient (C_L) and drag coefficient (C_D) for stationary cylinder are shown in Fig. 4 for 5 seconds of flow time. It must be noted that the frequency ratio for stationary cylinder is zero ($f/f_{vs} = 0$). The power spectral density (PSD) of the lift coefficient is also presented to show the natural frequency of vortex shedding (f_{vs}) at $Re = 100$. It is observed that the behavior of C_D and C_L is periodic. The PSD plot shows the frequency of vortex shedding by taking the fast Fourier transform (FFT) of the fluctuating lift coefficient. It is found that f_{vs} for the stationery cylinder is 2.5 Hz corresponding to Strouhal number (St) of 0.165.
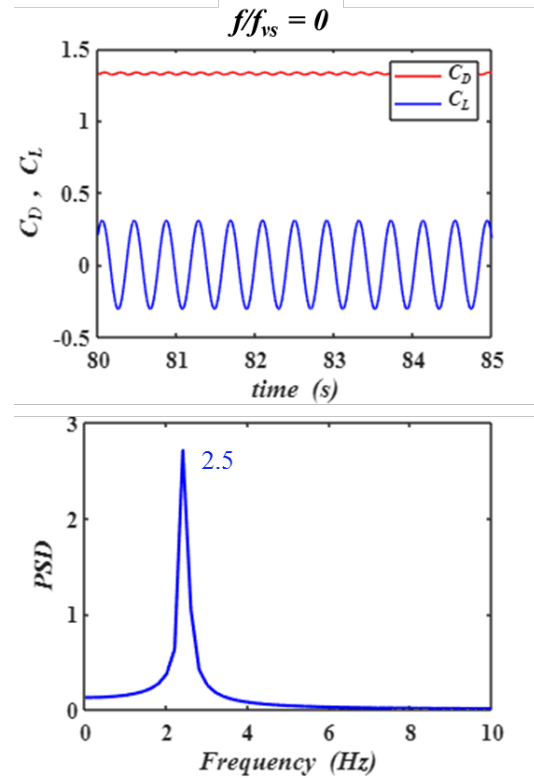

Fig. 4. Time histories of lift and drag coefficient (top), and power spectral density (bottom) of lift signal for stationary cylinder

The time histories of C_D and C_L for transversely oscillating cylinder at different frequency ratios (f/f_{vs}) are shown in Fig. 5. The record is shown for 5 seconds of the flow time. It is observed that the forcing frequency induces modulation in the lift and drag coefficient at frequency ratios of 0.5, 1.5, and 2. At $f/f_{vs} = 1$, frequency modulation does not occur, however the amplitude of C_D and C_L increases. This is because at $f/f_{vs} = 1$ lock-in occurs and the vibration frequency synchronizes with the vortex shedding frequency.

The frequency spectrum of the lift signals presented in Fig. 5 is shown in Fig. 6. The fast Fourier transform (FFT) of the signal is taken to obtain the power spectral density (PSD). At frequency ratio of 0.5, three distinct peaks are observed. The largest peak corresponds to the vortex shedding frequency (f_{vs}). However, the other two peaks correspond to the sum and difference of the forcing frequency and the vortex shedding frequency (f-f_{vs} and f+f_{vs}). This occurs as the forcing frequency interacts with the vortex shedding frequency. Only one peak is observed at frequency ratio of 1 as the forcing frequency synchronizes with the vortex shedding frequency and lock-in occurs. At frequency ratio of 1.5 and 2, two distinct peaks are observed. One for the vortex shedding frequency and the other for forcing frequency.
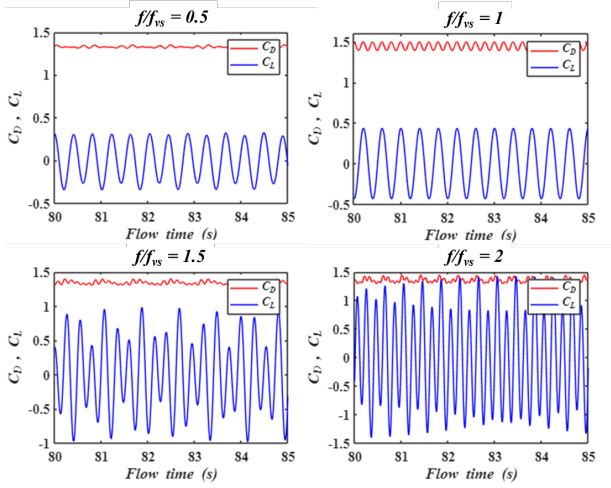
4

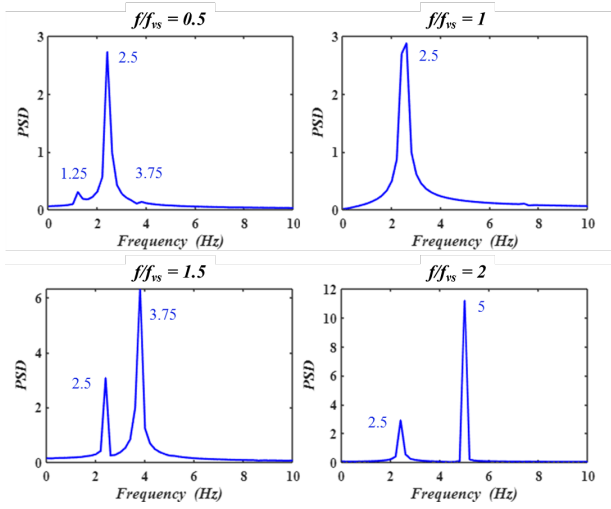**Fig. 5. Time histories of lift and drag coefficient at frequency ratio of 0.5, 1, 1.5, and 2.**

Fig. 6. Power spectral density (*PSD*) of the lift coefficient at frequency ratio of 0.5, 1, 1.5, and 2.

The average drag coefficient (C_D) and root mean square (*rms*) of lift coefficient (C_L) is shown in Fig. 7 at different frequency ratios. For the lift coefficient, *rms* of the signal is considered as the lift coefficient oscillates about zero mean therefore the average is always zero. Average C_D and *rms* of C_L for stationary cylinder ($f/f_{vs} = 0$) are also presented in Fig. 7 for comparison to the oscillating cylinder. Moving the cylinder at frequency ratio of 0.5 slightly increases the C_D and C_L however the increase is almost negligible. At $f/f_{vs} = 1$, a large increase in C_D is observed as the cylinder experiences lock-in condition. Lift coefficient also rises. Further increasing the frequency ratio increases the lift coefficient, however the drag coefficient appears to drop back to the original value of the stationary cylinder. The transverse oscillation of the cylinder has a significant effect on C_L however the effect on C_D is not prominent except for the lock-in condition.
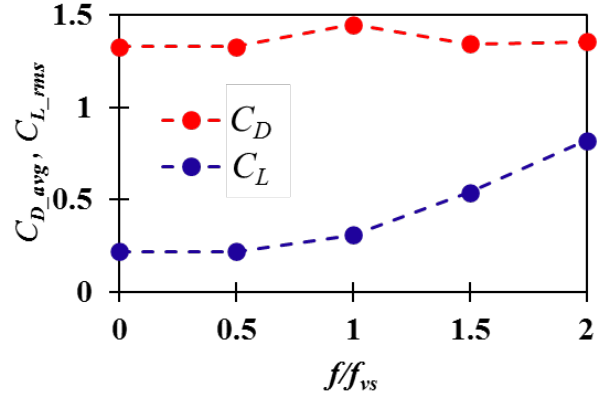

Fig. 7. Average drag coefficient and rms of lift coefficient at frequency ratio of 0, 0.5, 1, 1.5, and 2.

The vorticity contours shown in Fig. 8 look similar to each other for all frequency ratios. The 2S vortex shedding pattern is observed for all cases where two vortices of opposite sign are shed from the cylinder in one complete cycle of oscillation. The clockwise vortex shedding from top of the cylinder is displayed in red color whereas the anticlockwise vortex shedding from the bottom of the cylinder is shown in blue color.
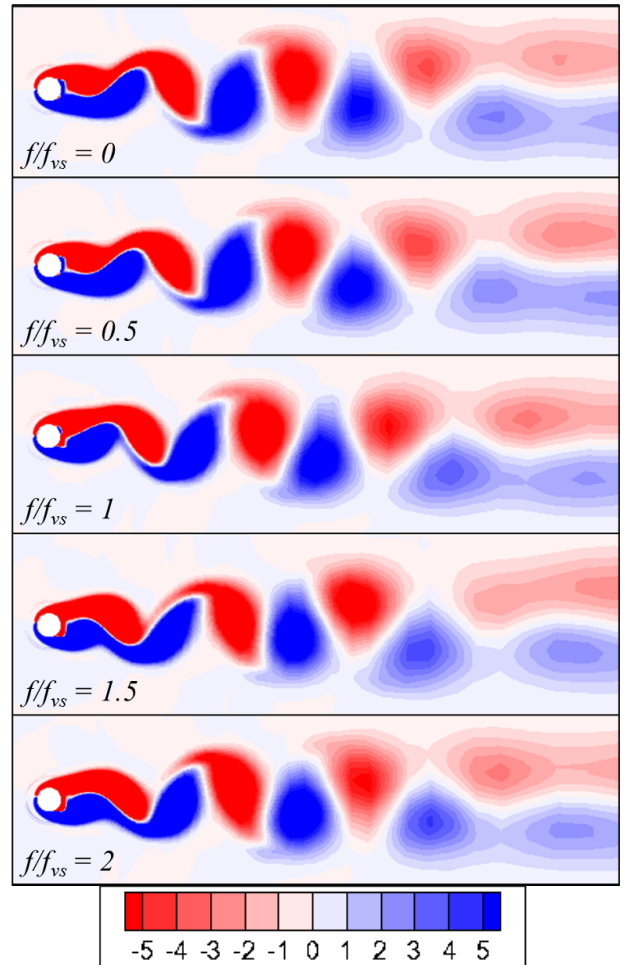

Fig. 8. Vorticity contours

4. Conclusion

The transverse oscillation of a circular cylinder at Reynolds number of 100 with different frequency ratios are numerically studied in this work. The time histories of lift and drag coefficient show that the cylinder oscillation causes modulation in amplitude and frequency of these coefficients. At frequency ratio of 1 lock-in occurs as the frequency of oscillation synchronizes with the natural vortex shedding frequency. Highest average drag is observed at this condition however the lift coefficient increases with increasing frequency ratio. The vorticity contours show the dominant 2S vortex shedding pattern for all the frequency ratios.

References

[1] Ali, U., Islam, Md., Janajreh, I., Fatt, Y., & Alam, Md. M. (2021). Flow-Induced Vibrations of Single and Multiple Heated Circular Cylinders: A Review. *Energies*, *14*(24), 8496. https://doi.org/10.3390/en14248496

[2] Derakhshandeh, J. F., & Alam, M. M. (2019). A review of bluff body wakes. Ocean Engineering, 182, 475–488. https://doi.org/10.1016/j.oceaneng.2019.04.093

[3] Ali, U., & Kamran, M. S. (2020). Geometric Optimization of a Gas Turbine Blade Cooling Passage using CFD. International Journal of Thermal and Environmental Engineering, 17(02). https://doi.org/10.5383/ijtee.17.02.004

[4] Hassan , H., Ait Abderrahmane, H., Ali, U., Islam, Md., & Janajreh, I. (2022). Numerical Analysis of Flow Over Slitted Cylinder and Experimental Validation using Soap-Film Technique. Proceedings of the ASME 2022 16th International Conference on Energy Sustainability (ES2022). Philadelphia, PA. July 11 – 13.

[5] Nakano, T., Fujisawa, N., Oguma, Y., Takagi, Y., & Lee, S. (2007). Experimental study on flow and noise characteristics of NACA0018 airfoil. Journal of Wind Engineering and Industrial Aerodynamics, 95(7), 511–531. https://doi.org/10.1016/j.jweia.2006.11.002

[6] Kuo, C.-H., & Hsieh, J. K. (2001). Unsteady flow structure and vorticity convection over the airfoil oscillating at high reduced frequency. Experimental Thermal and Fluid Science, 24(3–4), 117–129. https://doi.org/10.1016/S0894-1777(01)00044-9

[7] Ali, U., Modrek, M., Islam, M., & Janajreh, I. (2020). Numerical Study of Airfoil Shape and Blade Pitching on Vertical Axis Wind Turbine Through CFD Simulations. Volume 8: Energy, V008T08A060. https://doi.org/10.1115/IMECE2020-24003

[8] Gao, D.-L., Chen, W.-L., Li, H., & Hu, H. (2017). Flow around a slotted circular cylinder at various angles of attack. Experiments in Fluids, 58(10), 132. https://doi.org/10.1007/s00348-017-2417-8

[9] Abdi, R., Rezazadeh, N., & Abdi, M. (2019). Investigation of passive oscillations of flexible splitter plates attached to a circular cylinder. Journal of Fluids and Structures, 84, 302–317. https://doi.org/10.1016/j.jfluidstructs.2018.11.001

[10] Carberry, J., Sheridan, J., & Rockwell, D. (2001). Forces and Wake Modes of an Oscillating Cylinder. Journal of Fluids and Structures, 15(3–4), 523–532. https://doi.org/10.1006/jfls.2000.0363

[11] Roshko, A. (2003). On the development of turbulent wakes from vortex streets (Final) [California Institute of Technology; PDF]. https://doi.org/10.7907/4WDN-9807

[12] Williamson, C. H. K. (1996). Three-dimensional vortex dynamics in bluff body wakes. Experimental Thermal and Fluid Science, 12(2), 150–168. https://doi.org/10.1016/0894-1777(95)00085-2

[13] Ali, U., Islam, M., & Janajreh, I. (2021). Dynamic Behavior of a Streamwise Oscillating Heated Cylinder. ASME 2021 Heat Transfer Summer Conference, V001T01A009. https://doi.org/10.1115/HT2021-63856

[14] Ali, U., Islam, M., & Janajreh, I. (2021). Heated Circular Cylinder Subjected to Forced Spanwise Oscillations. Volume 7A: Dynamics, Vibration, and Control, V07AT07A036. https://doi.org/10.1115/IMECE2021-70713

[15] Sarpkaya, T. (2004). A critical review of the intrinsic nature of vortex-induced vibrations. Journal of Fluids and Structures, 19(4), 389–447. https://doi.org/10.1016/j.jfluidstructs.2004.02.005

[16] Wanderley, J. B. V., & Soares, L. F. N. (2015). Vortex-induced vibration on a two-dimensional circular cylinder with low Reynolds number and low mass-damping parameter. Ocean Engineering, 97, 156–164. https://doi.org/10.1016/j.oceaneng.2015.01.012

[17] Raghavan, K., & Bernitsas, M. M. (2011). Experimental investigation of Reynolds number effect on vortex induced vibration of rigid circular cylinder on elastic supports. Ocean Engineering, 38(5–6), 719–731. https://doi.org/10.1016/j.oceaneng.2010.09.003

[18] Chung, M.-H. (2016). Transverse vortex-induced vibration of spring-supported circular cylinder translating near a plane wall. European Journal of Mechanics - B/Fluids, 55, 88–103. https://doi.org/10.1016/j.euromechflu.2015.09.001

[19] Engelman, M. S., & Jamnia, M.-A. (1990). Transient flow past a circular cylinder: A benchmark solution. International Journal for Numerical Methods in Fluids, 11(7), 985–1000. https://doi.org/10.1002/fld.1650110706

[20] Prasanth, T. K., Behara, S., Singh, S. P., Kumar, R., & Mittal, S. (2006). Effect of blockage on vortex-induced vibrations at low Reynolds numbers. Journal of Fluids and Structures, 22(6–7), 865–876. https://doi.org/10.1016/j.jfluidstructs.2006.04.011

[21] Yang, Z., Ding, L., Zhang, L., Yang, L., & He, H. (2020). Two degrees of freedom flow-induced vibration and heat transfer of an isothermal cylinder. International Journal of Heat and Mass Transfer, 154, 119766. https://doi.org/10.1016/j.ijheatmasstransfer.2020.119766

[22] Kocabiyik, S., Mahfouz, F. M., & Al-Mdallal, Q. (2004). Numerical simulation of the flow behind a circular cylinder subject to small-amplitude recti-linear oscillations. Advances in Engineering Software, 35(10–11), 619–631. https://doi.org/10.1016/j.advengsoft.2004.06.005

[23] ANSYS Fluent theory guide

[24] Williamson, C. H. K. (1989). Oblique and parallel modes of vortex shedding in the wake of a circular cylinder at low Reynolds numbers. Journal of Fluid Mechanics, 206, 579–627. https://doi.org/10.1017/S0022112089002429